

Room temperature optically pumped GeSn microdisk lasers

Cite as: Appl. Phys. Lett. **120**, 051107 (2022); <https://doi.org/10.1063/5.0074478>

Submitted: 08 October 2021 • Accepted: 24 January 2022 • Published Online: 02 February 2022

 J. Chrétien,  Q. M. Thai,  M. Frauenrath, et al.



View Online



Export Citation



CrossMark

ARTICLES YOU MAY BE INTERESTED IN

[Colloidal II–VI–Epitaxial III–V heterostructure: A strategy to expand InGaAs spectral response](#)
Applied Physics Letters **120**, 051101 (2022); <https://doi.org/10.1063/5.0076708>

[Transparent ultrathin Ag nanomesh electrode fabricated by nanosphere lithography for organic light-emitting devices](#)

Applied Physics Letters **120**, 051106 (2022); <https://doi.org/10.1063/5.0079505>

[Perspective on scalable high-energy-density polymer dielectrics with ultralow loadings of inorganic nanofillers](#)

Applied Physics Letters **120**, 050502 (2022); <https://doi.org/10.1063/5.0080825>

 QBLOX



1 qubit

Shorten Setup Time

Auto-Calibration

More Qubits

Fully-integrated

Quantum Control Stacks

Ultrastable DC to 18.5 GHz

Synchronized <<1 ns

Ultralow noise



100s qubits

[visit our website >](#)

Room temperature optically pumped GeSn microdisk lasers

Cite as: Appl. Phys. Lett. **120**, 051107 (2022); doi: [10.1063/5.0074478](https://doi.org/10.1063/5.0074478)

Submitted: 8 October 2021 · Accepted: 24 January 2022 ·

Published Online: 2 February 2022









View Online



Export Citation



CrossMark

J. Chrétien,^{1,a)}  Q. M. Thai,¹  M. Frauenrath,²  L. Casiez,²  A. Chelnokov,²  V. Reboud,²  J. M. Hartmann,² M. El Kurdi,³ N. Pauc,¹ and V. Calvo¹

AFFILIATIONS

¹University Grenoble Alpes, CEA, Grenoble INP, IRIG, PHELIQS, Grenoble, France

²University Grenoble Alpes, CEA, LETI, Grenoble, France

³Université Paris-Saclay, CNRS, C2N, 10 boulevard Thomas Gobert, 91120 Palaiseau, France

^{a)} Author to whom correspondence should be addressed: jeremie.chretien@outlook.com

ABSTRACT

GeSn alloys are promising materials for light emitters monolithically grown on silicon. In this work, we demonstrate room temperature (RT) lasing in a GeSn hetero-structure with 17.2% of Sn. We report a threshold of 3.27 MW cm^{-2} at 305 K with peak emission at 353 meV. We ascribe these improvements to a higher tin concentration in the GeSn active layer with lower Sn content barriers on each side and to a better thermal dissipation provided by an adapted pedestal architecture beneath the GeSn micro-disk. This outcome is a major milestone for a fully integrated group-IV semiconductor laser on Si.

Published under an exclusive license by AIP Publishing. <https://doi.org/10.1063/5.0074478>

GeSn materials are appealing candidates for many applications, ranging from photodetectors^{1–3} to molecular spectroscopy and gas sensing in the mid-infrared (2–5 μm). However, they are still behind III–V counterparts in terms of lasing performance (laser threshold and maximum lasing temperature), even if recent progress in GeSn doping yielded the first electrically pumped GeSn laser with a limited temperature of 100 K.⁴ According to theoretical works,^{5,6} the maximum operating laser temperature is dependent on the energy offset between Γ and L valleys. High Sn contents and high amounts of tensile strain are two strategies that can be leveraged to increase the energy offset between the Γ and L valleys and enhance the optical gain through a carrier density increase in the Γ valley. Experimental efforts were spent since the early 2010s to increase the Sn concentration (over 8%) in GeSn alloys and have a direct bandgap, which are mandatory for stimulated light emission. Since the first demonstration, in 2015, of lasing up to 90 K (Ref. 7) in a Fabry–Pérot (FP) cavity with its core at a thick GeSn layer with 12.6% of Sn (called “GeSn 12.6%” from now on), the maximum operating temperature has steadily improved from 180 up to 270 K by increasing the Sn concentration from 16% up to 20%, using FP^{8–10} or relaxed microdisk cavities.^{11–13} Inserting the active layer between lower Sn content layers was also shown to improve the lasing performance.^{12,13} Tensile strain engineering was also investigated to increase the maximum lasing temperature. It resulted in a maximum lasing temperature of 273 K for tensile strained

GeSn 16% suspended microbridges¹⁴ with a high laser threshold of 2 MW cm^{-2} , however. Lasing under continuous-wave optical pumping was also demonstrated in 5.4% Sn bi-dimensionally tensile strained microdisks¹⁵ with removal of Ge/GeSn interfacial dislocations during layer transfer.

Room temperature (RT) lasing in GeSn is, thus, closely dependent on the interplay between a relatively high laser threshold near RT and the dissipation of heat generated in the resonators.¹⁶ Decreasing thresholds could help in reaching RT operation, even in non-thermally optimized devices. Here, we demonstrate RT lasing in Sn rich layers sandwiched between lower Sn content layers with an improved heat transfer scheme and without the help of tensile strain.

The 1080 nm thick GeSn heterostructure was grown in a 200 mm Epi Centura 5200 reduced pressure-chemical vapor deposition cluster tool from Applied Materials on top of a 2.5 μm thick Ge strain relaxed buffer (SRB), itself grown on the (001) Si substrate. Ge_2H_6 , SnCl_4 , and Si_2H_6 were used as precursor gases. A step graded Sn concentration approach was adopted here with constant Ge_2H_6 and SnCl_4 flows and temperatures, which gradually decreased from 349 °C down to 307 °C during growth at 100 Torr, as described in Ref. 17. The thick, optically active GeSn 17.2% layer grown at 307 °C was capped at 313 °C by GeSn 16.1% and 14.1% layers. The Sn concentration lowering, from 16.1% down to 14.1%, was achieved through a reduction of the SnCl_4 flow. Reducing the Sn content by lowering the SnCl_4 flow instead of

increasing the growth temperature reduced the risk of having Sn surface segregation/precipitation. The Sn contents and the macroscopic degrees of strain relaxation of the various GeSn layers were determined experimentally thanks to the Reciprocal Space Map around the (224) asymmetric x-ray diffraction (XRD) order shown in Fig. 1(a). Data are gathered in Table S1. The optically active part of the heterostructure was made up of a ~ 430 nm GeSn 17.2% \pm 0.3% optically active layer sandwiched in-between ~ 110 nm thick GeSn 16.1% \pm 0.3% barriers, themselves embedded in ~ 110 nm thick GeSn 14.1% \pm 0.3% layers [stack schematics in Fig. 1(a)].

The as-grown GeSn stack shows maximum peak emission at 0.406 eV (3052 nm) at 25 K and under continuous wave optical pumping, as shown in Fig. 1(b), indicating a higher Sn concentration in the active GeSn layer than in Ref. 13 with a photoluminescence peak located at 0.428 eV (2900 nm) at 15 K. This emission wavelength is in good agreement with the 17.2% Sn content obtained in XRD. Two sets of resonators were fabricated from the very same heterostructure. The final microdisks did not differ in terms of an optically active stack. They were drastically different in terms of the thermal management strategy, however. Dimensions and underlying pedestals were indeed not the same. Sample 1 was obtained via anisotropic and isotropic dry etching of the blanket stack in a similar approach to previous works.^{12,18} The final thickness of the GeSn stack after isotropic buffer etching was ~ 900 nm, corresponding (from the bottom to the top) to

the GeSn 14.1%, 16.1%, 17.2%, 16.1%, and 14.1% layers in Fig. 1(a) schematics. The heavily dislocated GeSn 7.4% and the “transition layer” were removed during fabrication. Sample 2 was obtained following the steps presented in Fig. 1(c). It was made of the as-grown stack (sample A) bonded upside-down on a host pedestal (sample B). To that end, a 500 nm thick AlN layer was sputter deposited on sample A, followed by a 40 nm-10 nm-200 nm thick TiN-Cr-Au trilayer. TiN is indeed expected to reduce metallic diffusion taking place in the metallic bonding step that follows, as this material is known for its diffusion barrier properties.¹⁹ Sample A and sample B surfaces were then placed face to face with a small In layer sandwiched between the two samples then annealed at a temperature around 160–180 °C. An InAu alloy, with a high In concentration, formed upon cooling, creating a solder between samples A and B.²⁰ The backside of sample A was then removed with first some polishing followed by selective SF_6 -based dry etching of the last tens of μm of the Si substrate, the whole Ge buffer, and the low Sn content GeSn layers, leaving intact the high Sn content GeSn layers underneath. The final stack thickness was 770 nm, corresponding to (from the end sample’s bottom to the top) the GeSn 14.1%, 16.1%, 17.2%, and 16.1% layers. E-beam lithography and anisotropic etching steps were then used. Microdisks were underetched over 2 μm by dipping samples in a 326MIF developer, an aqueous developer containing tetramethylammonium hydroxide, during 40 min, with afterwards a rinse in de-ionized water. The choice of the

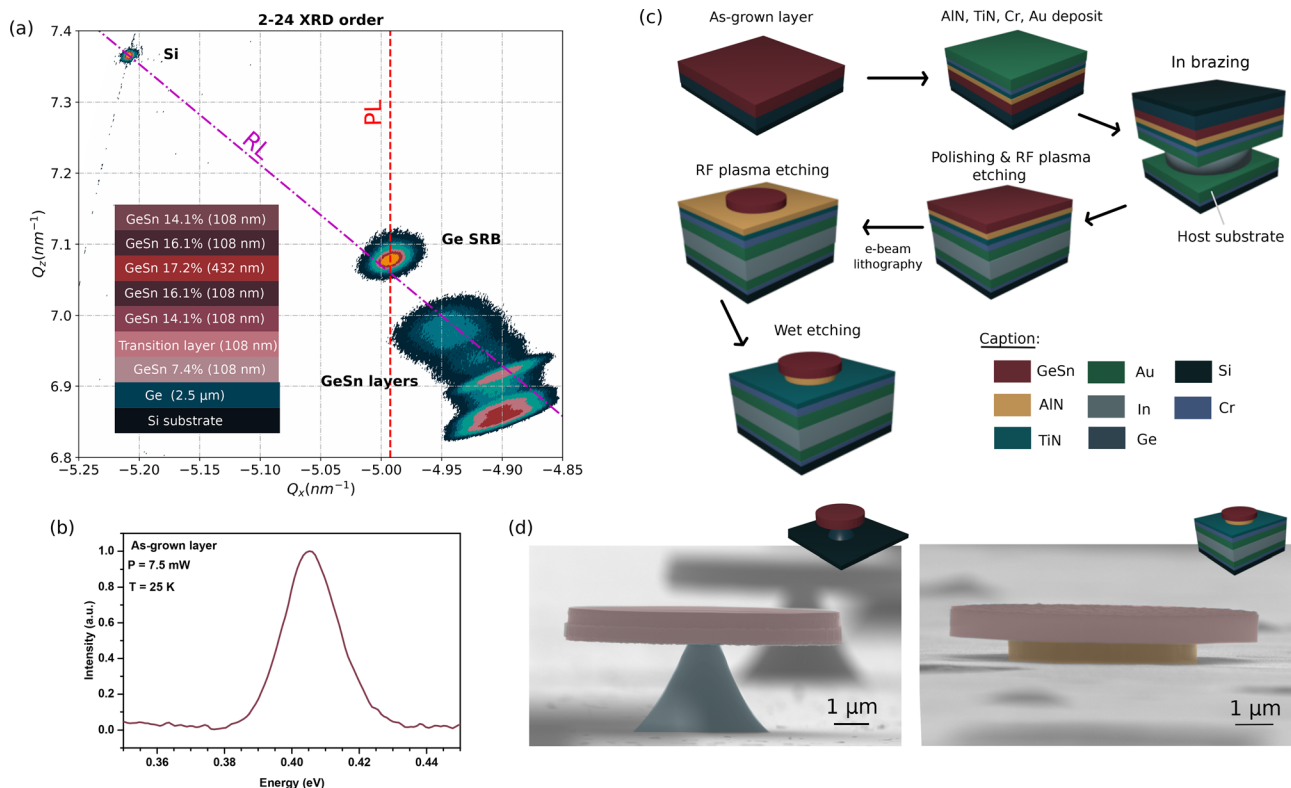


FIG. 1. (a) Reciprocal space map around the (224) XRD asymmetric reflection for the GeSn 17.2% heterostructure epitaxially grown on a 2.5 μm thick Ge SRB, itself on a Si (001) substrate (layer stack shown in the inset). (b) Photoluminescence spectrum of the as-grown stack at 25 K. (c) Sketch of the different steps of the GeSn layer transfer with indium brazing. (d) Scanning electron microscopy images of 8 μm diameters GeSn microdisks on Ge (left) and AlN (right) pedestals.

bonding strategy was dictated here by the bonding temperature, which had to be kept as low as possible to avoid Sn segregation/precipitation in the GeSn layers. This phenomenon is known to happen at temperatures close to the growth temperature,²¹ which was 307 °C only for the 17.2% layer.

A recent work²² on the thermal properties of GeSn alloys showed a conductivity drop as the Sn content increased from 58 W m⁻¹ K⁻¹ (Ref. 23) (pure Ge) down to 4 W m⁻¹ K⁻¹ only (for GeSn 14%). Thus, heat transport in GeSn microdevices is expected to be hindered compared with their pure Ge counterparts. The dissipation of the laser induced heating from the GeSn microdisk to the substrate is dependent on (i) the nature and the thickness of the pedestal, (ii) the underetching, and (iii) the suspended GeSn active area. GeSn epilayers are traditionally grown on top of thick (2.5 μm) Ge strain-relaxed buffers, themselves on Si substrates, minimizing the amount of misfit dislocations in the GeSn layers. Playing on the heat transport properties of this thermal sink adds an extra lever to mitigate the heat of the gain medium under very high pump power, near RT. Changing the thermal conductivity of the pedestal material, by replacing Ge [$k_{Ge} = 58 \text{ W} \cdot \text{m}^{-1} \text{ K}^{-1}$ (Ref. 23)] with AlN [$k_{AlN} = 285 \text{ W} \cdot \text{m}^{-1} \text{ K}^{-1}$ (Ref. 23)], increases the heat flux toward the substrate. Thinning down the pedestal by 5 (from 2.5 μm for Ge to 0.5 μm for AlN) and increasing the heat exchange area at the disk

pedestal interface drastically decrease the pedestal's thermal resistance. Reducing the disk undercut while avoiding mode overlap with the pedestal also reduces the thermal resistance contribution from the crown shaped region between the undercut line and the modal region. A thin AlN pedestal with a short undercut, thus, offers, in principle, a better alternative to Ge, mostly used to date, for heat evacuation. Thick Ge buffers are indeed necessary to grow high quality GeSn epilayers. In addition, AlN is a wideband gap semiconductor, which does not absorb infrared radiation, preventing any mode overlap loss with the pedestal.

In the following, we compare 15 μm diameter microdisk lasers on (i) a Ge pedestal (with a 2.5 μm pedestal thickness and 3.5 μm under-etches) and (ii) an AlN pedestal (with a 0.54 μm pedestal thickness and 1.55 μm under-etches). We show that lasing performances are better for the latter. We estimate the modal confinement factors to be 69.6% for the disk on AlN and 66.2% for the disk on Ge. In addition, there are no noticeable layer bending for both types of disks. Given that radii are the same and confinement factors are very close, we, thus, expect photon propagation conditions to be the same in both types of disks. It is important to note that the step graded approach concentrates the dislocations in the low Sn content layers, etched in both samples, and that the active 17.2% medium along its interfaces is preserved for both configurations. This is in sharp contrast with previous work,²⁴ where severe

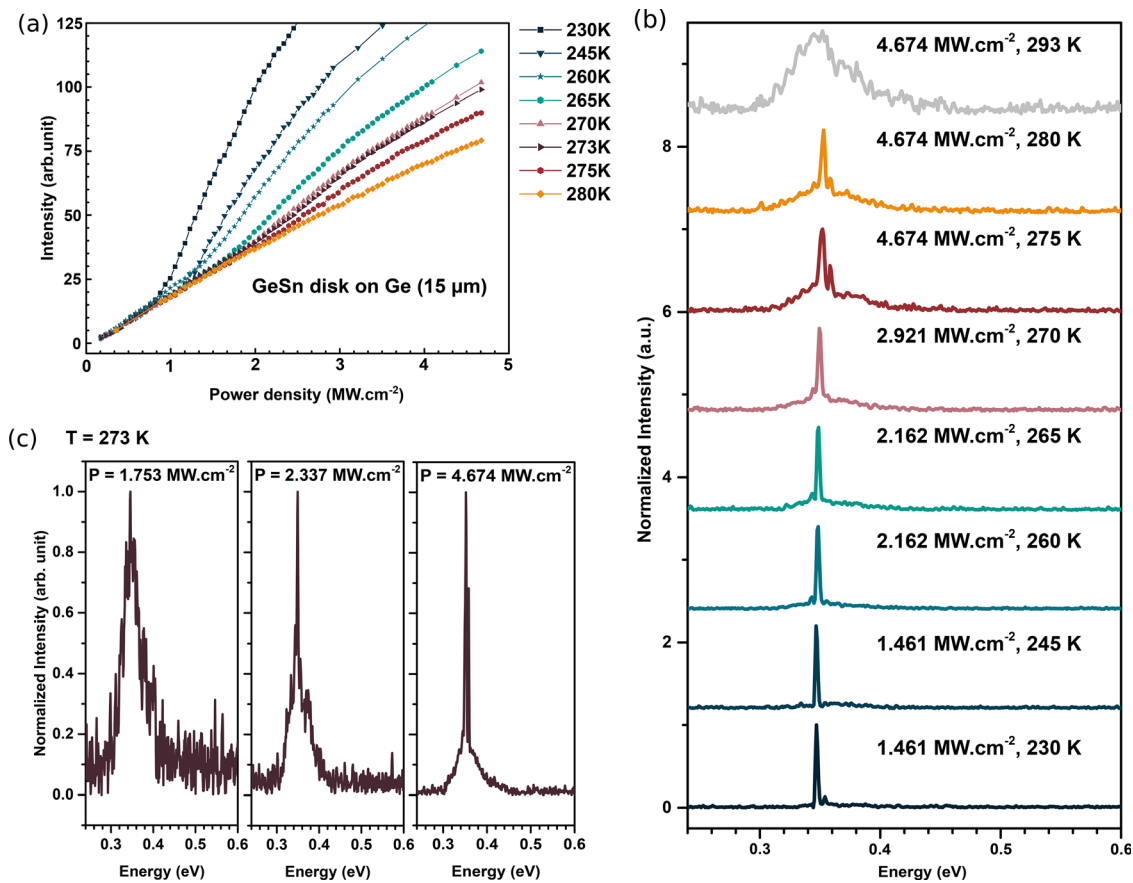


FIG. 2. (a) L-L curves at different temperatures from 230 up to 280 K and (b) corresponding temperature-dependent spectra for a 15 μm diameter GeSn microdisk on a Ge pedestal. (c) Spectra at 273 K under a pulsed density power excitation of 1.753 (under the threshold), 2.337 (near the threshold), and 4.674 MW cm⁻² (above the threshold).

non-radiative recombination by interface defects in the active medium directly grown onto the Ge buffer was mitigated by GeSn bonding and partial back etching of the defective part of the active medium at different degrees after GeSn bonding in GeSnOI or underetching in microdisks on Ge structures. Here, the recombination activity not only near the mode area but also the strain state (relaxed) and photon propagation properties in the gain medium are similar for both samples. This makes heat conduction properties the main discriminating mechanism with differences not only in heat conduction properties arising from different thermal resistances in the pedestals but also and more importantly in the undercut resistance rather high for these concentrations (see the [supplementary material](#)), which depends not only on its length but also on the GeSn conductivity.

A pulsed 1064 nm Nd:YAG laser, with a 0.6 ns pulse duration and a repetition rate of 50 kHz, was used to optically pump the GeSn microdisks. The laser beam was focused on the sample in a 25 μm

diameter circular spot with a 13.8 \times magnification Cassegrain objective. The backscattered PL signal was analyzed with a Fourier transform infrared interferometer equipped with an InSb detector. [Figure 2](#) shows the optical characterization of a 15 μm diameter GeSn microdisk on a Ge pedestal. Light in–light out (L–L) curves for several temperatures are presented in [Fig. 2\(a\)](#). We clearly observed slope breaks from 230 up to 275 K with a laser threshold increase from 791 kW cm^{-2} up to 2.54 MW cm^{-2} , respectively.²⁵ Lasing spectra are shown in [Fig. 2\(b\)](#) as a function of the temperature. A single mode can be observed at 230 K with photon energies around 0.347 eV. Spectra acquired below, near, and above the threshold at 273 K are provided in [Fig. 2\(c\)](#). The mode is still visible at 280 K, but the corresponding L–L curve does not show a slope break anymore.

A 15 μm diameter GeSn microdisk on an AlN pedestal was otherwise investigated. [Figure 3\(a\)](#) shows photoluminescence spectra at various temperatures ranging from 230 to 308 K. The maximum lasing

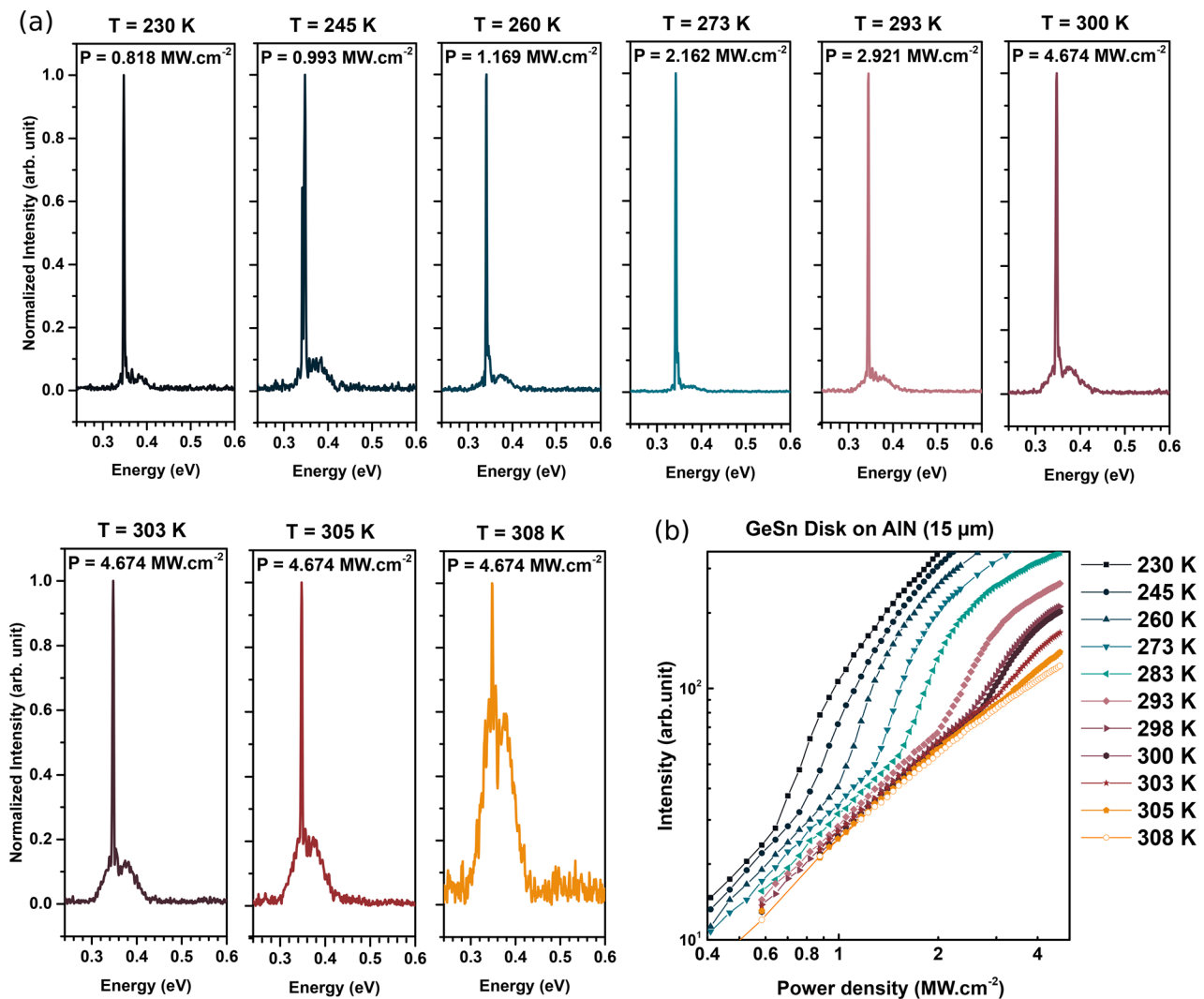


FIG. 3. (a) Spectra of a 15 μm diameter GeSn microdisk resonator on an AlN pedestal from 230 up to 308 K. (b) L–L curves for the same temperature range.

temperature was improved up to 305 K compared to the Ge case. A strong single lasing mode is clearly visible at 0.348 eV, i.e., at nearly the same energy than for the micro-disk on a Ge pedestal. It should be noted that spontaneous emission at 0.38 eV is still significant even at 273 K. We attribute this contribution to the AlN pedestal, since its low refractive index (around 2) increases the interface reflection coefficient compared to the Ge pedestal. It results in an enhancement of the PL signal at the center of the microdisk. The ratio between the lasing peak and spontaneous PL maxima, however, drops from 54 down to 5 when the temperature increases from 273 up to 305 K. The lasing

mode disappears at 308 K. L-L curves are plotted in Fig. 3(b) for temperatures in the 230–308 K range.

From 230 to 305 K, we clearly observe both the optical mode and the nonlinearity of the L-L curve, which sets an upper lasing limit between 305 and 308 K.

Figure 4(a) shows the experimental thresholds $P_{th}(T)$ for both types of microdisks as a function of the temperature (Ge pedestal: blue full squares and AlN pedestal: red full circles). Lasing thresholds were, in Figs. 2(a) and 3(b), power densities at which there were slope breaks in the L-L curves. Extracted data show a biexponential behavior,

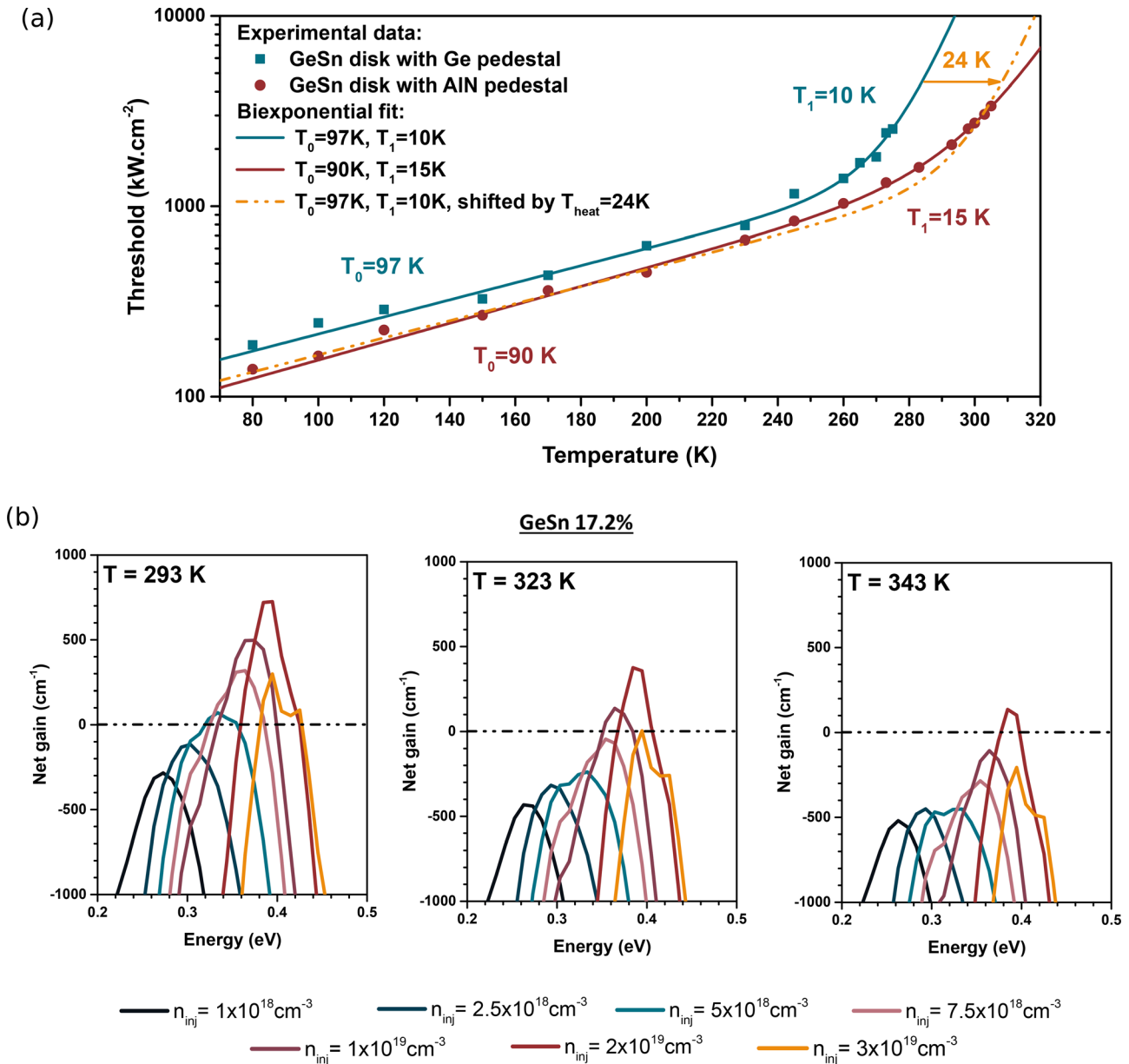


FIG. 4. (a) Threshold as a function of the temperature for 15 μ m diameter GeSn disks on Ge (blue full squares) and AlN (red full circles) pedestals. (b) Computed net gain of GeSn 17.2% as a function of the photon energy at different values of n_{inj} between 1×10^{18} and 3×10^{19} cm⁻³ calculated for 293, 323, and 343 K.

$P_{th}(T) = P_0 \exp\left(\frac{T}{T_0}\right) + P_1 \exp\left(\frac{T}{T_1}\right)$ with $T_0^{Ge} = 97$ K, $T_1^{Ge} = 10$ K and $T_0^{AlN} = 90$ K, $T_1^{AlN} = 15$ K. Similar characteristic temperatures in both samples reveal identical processes for gain loss with temperature (thermal broadening of carriers in the bands, thermal escape from the barriers, Auger recombination...) as a consequence of the basically identical nature of the gain medium and its environment. The thermal shift between both curves is slightly power dependent, and a mean shift of 24 K (see the dotted curve) is deduced by fitting the AlN data with the Ge parameters while introducing a thermal shift as the only fitting parameter in the biexponential law. This is definitely indicative of overheating of the gain medium in the Ge pedestal case compared to the AlN pedestal case. At 230 K, a roll-off is only observed on the L-L curve of the Ge pedestal case (see the [supplementary material](#)), indicating heating of the device contrary to the AlN pedestal case. For the highest temperatures, diffusion of carriers from the modal to the inner zone might induce extra electronic losses through escape to the unattacked and defective low tin content layers in the pedestal of the microdisk on Ge and could contribute to slight increase in the threshold. RT lasing operation in our free-standing system is, thus, made possible by changing the pedestal architecture.

We performed theoretical calculations of the optical gain near RT. The simulation methodology was described in detail in Ref. 6. It takes into account contributions from the interband transition—i.e., from valence bands (VBs) to conduction bands (CBs), the intervalence band transition (VB–VB), and the free carrier absorption (FCA—using the empirical formula established by Liu *et al.* for Ge,²⁶ and extended here for GeSn). We plot in Fig. 4(b) the net gain as a function of the photon energy for GeSn 17.2% at different values of n_{inj} between 1×10^{18} and 3×10^{19} cm⁻³ and for three temperatures: 293, 323, and 343 K. At 293 K, i.e., the cryostat temperature, a robust net gain (300 cm⁻¹) is reached for $n_{inj} = 7.5 \times 10^{18}$ cm⁻³. The maximum of the net gain curve is 750 cm⁻¹ for $n_{inj} = 2 \times 10^{19}$ cm⁻³. It progressively drops by a factor of two between 293 and 323 K and vanishes for T = 343 K. Furthermore, increasing the Sn content leads to maximizing the net gain at room temperature and above, as pointed out in Ref. 6, where an optimum of the concentration for maintaining positive net gains at RT is found for Sn rich layers.

We have just shown that effective temperatures were different for AlN and Ge pedestals (24 K, experimentally). Because of laser heating, they were also different from the cryostat temperature. The thermal profile at the steady-state was also derived from finite element method (FEM) simulations (the [supplementary material](#)). Simulation showed that the disk underetch, i.e., the suspended active zone, was a key parameter to be tuned to cooldown the laser cavity. Taking into account pump-laser overheating and the computed optical gain, we could expect to have lasing at even higher temperatures for better cooled cavities like pillar or released microdisks on a thermal conductive layer, which leads to the same conclusion of Kim *et al.*²⁷

To conclude, we demonstrated lasing in a 17.2% GeSn microdisk under optical pumping up to 305 K in strain free, underetched microdisks on pedestals. By changing the pedestal architecture, we managed to have room temperature lasing, a significant milestone for industrial applications. We estimated that such thermally optimized GeSn layers have the potential to lase up to 330–340 K without strain assistance. Such results are very promising for group-IV light emitters and could be improved via thermal and tensile strain management.

See the [supplementary material](#) for more information on reciprocal space mapping, thermal simulations, the optical spectrum, and gain computations.

This work was supported by the Elegante ANR Project and Gelato Carnot Project. The authors acknowledge the assistance of the staff belonging to CEA-LETI's clean rooms and CEA Advanced technological platform (PTA). They are also grateful for help during GeSn morphological characterization experiments.

AUTHOR DECLARATIONS

Conflict of Interest

The authors have no conflicts to disclose.

DATA AVAILABILITY

The data that support the findings of this study are available from the corresponding author upon reasonable request.

REFERENCES

- A. Gassenq, F. Gencarelli, J. V. Campenhout, Y. Shimura, R. Loo, G. Narcy, B. Vincent, and G. Roelkens, *Opt. Express* **20**, 27297 (2012).
- M. R. M. Atalla, S. Assali, A. Attiaoui, C. Lemieux-Leduc, A. Kumar, S. Abdi, and O. Moutanabbir, *Adv. Funct. Mater.* **31**, 2006329 (2021).
- H. Tran, T. Pham, J. Margetis, Y. Zhou, W. Dou, P. C. Grant, J. M. Grant, S. Al-Kabi, G. Sun, R. A. Soref, J. Tolle, Y.-H. Zhang, W. Du, B. Li, M. Mortazavi, and S.-Q. Yu, *ACS Photonics* **6**, 2807 (2019).
- Y. Zhou, Y. Zhou, Y. Miao, S. Ojo, S. Ojo, H. Tran, G. Abernathy, G. Abernathy, J. M. Grant, J. M. Grant, S. Amoah, G. Salamo, G. Salamo, W. Du, J. Liu, J. Margetis, J. Tolle, Y. Zhang, G. Sun, R. A. Soref, B. Li, S.-Q. Yu, and S.-Q. Yu, *Optica* **7**, 924 (2020).
- D. Rainko, Z. Ikonik, A. Elbaz, N. von den Driesch, D. Stange, E. Herth, P. Boucaud, M. E. Kurdi, D. Grützmacher, and D. Buca, *Sci. Rep.* **9**, 259 (2019).
- Q. M. Thai, J. Chretien, M. Bertrand, L. Casiez, A. Chelnokov, V. Reboud, N. Pauc, and V. Calvo, *Phys. Rev. B* **102**, 155203 (2020).
- S. Wirths, R. Geiger, N. von den Driesch, G. Mussler, T. Stoica, S. Mantl, Z. Ikonik, M. Luysberg, S. Chiussi, J. M. Hartmann, H. Sigg, J. Faist, D. Buca, and D. Grützmacher, *Nat. Photonics* **9**, 88 (2015).
- S. Al-Kabi, S. A. Ghetmiri, J. Margetis, T. Pham, Y. Zhou, W. Dou, B. Collier, R. Quinde, W. Du, A. Mosleh, J. Liu, G. Sun, R. A. Soref, J. Tolle, B. Li, M. Mortazavi, H. A. Naseem, and S.-Q. Yu, *Appl. Phys. Lett.* **109**, 171105 (2016).
- J. Margetis, S. Al-Kabi, W. Du, W. Dou, Y. Zhou, T. Pham, P. Grant, S. Ghetmiri, A. Mosleh, B. Li, J. Liu, G. Sun, R. Soref, J. Tolle, M. Mortazavi, and S.-Q. Yu, *ACS Photonics* **5**, 827 (2018).
- Y. Zhou, W. Dou, W. Du, S. Ojo, H. Tran, S. A. Ghetmiri, J. Liu, G. Sun, R. Soref, J. Margetis, J. Tolle, B. Li, Z. Chen, M. Mortazavi, and S.-Q. Yu, *ACS Photonics* **6**, 1434 (2019).
- D. Stange, S. Wirths, R. Geiger, C. Schulte-Braucks, B. Marzban, N. von den Driesch, G. Mussler, T. Zabel, T. Stoica, J.-M. Hartmann, S. Mantl, Z. Ikonik, D. Grützmacher, H. Sigg, J. Witzens, and D. Buca, *ACS Photonics* **3**, 1279 (2016).
- V. Reboud, A. Gassenq, N. Pauc, J. Aubin, L. Milord, Q. M. Thai, M. Bertrand, K. Guillois, D. Rouchon, J. Rothman, T. Zabel, F. Armand Pilon, H. Sigg, A. Chelnokov, J. M. Hartmann, and V. Calvo, *Appl. Phys. Lett.* **111**, 092101 (2017).
- Q. M. Thai, N. Pauc, J. Aubin, M. Bertrand, J. Chretien, V. Delaye, A. Chelnokov, J.-M. Hartmann, V. Reboud, and V. Calvo, *Opt. Express* **26**, 32500 (2018).
- J. Chretien, N. Pauc, F. Armand Pilon, M. Bertrand, Q.-M. Thai, L. Casiez, N. Bernier, H. Dansas, P. Gergaud, E. Delamadeleine, R. Khazaka, H. Sigg, J. Faist, A. Chelnokov, V. Reboud, J.-M. Hartmann, and V. Calvo, *ACS Photonics* **6**(10), 2462–2469 (2019).
- A. Elbaz, D. Buca, N. von den Driesch, K. Pantzas, G. Patriarche, N. Zerounian, E. Herth, X. Checoury, S. Sauvage, I. Sagnes, A. Foti, R. Ossikowski, J.-M.

- Hartmann, F. Boeuf, Z. Ikonic, P. Boucaud, D. Grützmacher, and M. E. Kurdi, *Nat. Photonics* **14**, 375–382 (2020).
- ¹⁶D. Burt, H.-J. Joo, Y. Jung, Y. Kim, M. Chen, Y.-C. Huang, and D. Nam, *Opt. Express* **29**, 28959 (2021).
- ¹⁷J. Aubin, J. M. Hartmann, A. Gassenq, J. L. Rouviere, E. Robin, V. Delaye, D. Cooper, N. Mollard, V. Reboud, and V. Calvo, *Semicond. Sci. Technol.* **32**, 094006 (2017).
- ¹⁸S. Gupta, R. Chen, Y.-C. Huang, Y. Kim, E. Sanchez, J. S. Harris, and K. C. Saraswat, *Nano Lett.* **13**, 3783 (2013).
- ¹⁹W. E. Martinez, G. Gregori, and T. Mates, *Thin Solid Films* **518**, 2585 (2010).
- ²⁰W. W. So and C. C. Lee, *IEEE Trans. Comp. Packag. Technol.* **23**, 377 (2000).
- ²¹P. Zaumseil, Y. Hou, M. A. Schubert, N. von den Driesch, D. Stange, D. Rainko, M. Virgilio, D. Buca, and G. Capellini, *APL Mater.* **6**, 076108 (2018).
- ²²D. Spirito, N. von den Driesch, C. L. Manganelli, M. H. Zoellner, A. A. Corley-Wiciak, Z. Ikonic, T. Stoica, D. Grützmacher, D. Buca, and G. Capellini, *ACS Appl. Energy Mater.* **4**(7), 7385–7392 (2021).
- ²³Ioffe Institute, see <http://www.ioffe.ru/SVA/> for “New Semiconductor Materials. Characteristics and Properties” (2020).
- ²⁴B. Wang, E. Sakat, E. Herthl, M. Gromovyi, A. Bjelajac, J. Chaste, G. Patriarche, P. Boucaud, F. Boeuf, N. Pauc, V. Calvo, J. Chrétien, M. Frauenrath, A. Chelnokov, V. Reboud, J.-M. Hartmann, and M. El Kurdi, *Light: Sci. Appl.* **10**, 232 (2021).
- ²⁵“Scrutinizing lasers,” *Nat. Photonics* **11**, 139 (2017).
- ²⁶J. Liu, X. Sun, D. Pan, X. Wang, L. C. Kimerling, T. L. Koch, and J. Michel, *Opt. Express* **15**, 11272 (2007).
- ²⁷Y. Kim, S. Assali, D. Burt, Y. Jung, H.-J. Joo, M. Chen, Z. Ikonic, O. Moutanabbir, and D. Nam, *Adv. Opt. Mater.* **10**, 2101213 (2022).